Environmental Science & Technology

Article

Cite This: Environ. Sci. Technol. 2019, 53, 14348−14356

pubs.acs.org/est

Nitrous Oxide and Methane Dynamics in Woodchip Bioreactors: Effects of Water Level Fluctuations on Partitioning into Trapped Gas Phases

Philip M. McGuire and Matthew R. Reid*

School of Civil and Environmental Engineering, Cornell University, Ithaca, New York 14853, United States

* Supporting Information

ABSTRACT: Woodchip bioreactors (WBRs) are low-cost, passive systems for nonpoint source nitrogen removal at terrestrial−aquatic interfaces. The greenhouse gases nitrous oxide (N_2O) and methane (CH_4) can be produced within WBRs, and efforts to reduce N_2O and CH_4 emissions from WBR systems require improved understanding of the biogeochemical and physical−chemical mechanisms regulating their production, transport, and release. This study evaluates the impact of trapped gas-filled void volume as sinks of dissolved gases from water and as sources of episodic fluxes when water levels fall. Dissolved gas tracer experiments in a laboratory bioreactor were used to parameterize nonequilibrium advection-dispersion-gas transfer models and quantify trapping of gas-filled voids as a function of antecedent hydrological conditions. Experiments following a water-level rise revealed that up to 24% of the WBR pore volume was occupied by trapped gas phases, which were primarily located in pore spaces inside woodchips. This finding was confirmed with X-ray-computed microtomography. N_2O (3.3−10%) and CH_4 (4.3−14%) injected into the reactor following a water table rise partitioned into gas-filled voids and were released when water tables fell. In the case of N_2O, partitioning into trapped gas phases makes N_2O unavailable for enzymatic reduction, potentially enhancing N_2O fluxes under fluctuating water levels.

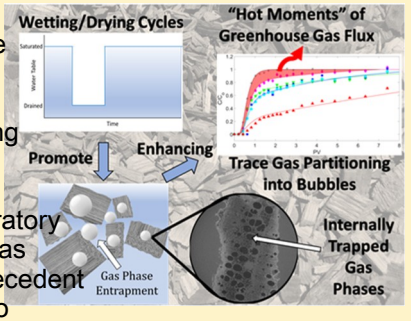

1. INTRODUCTION

Approximately one-quarter of all nitrogen (N) applied to terrestrial systems crosses the terrestrial−aquatic interface into surface waters,[1] making ecosystems at land-water boundaries critical buffer zones for controlling N release to aquatic environments. Environments at land-water boundaries are protected and/or engineered to enhance denitrification, the biologically mediated reduction of nitrate (NO_3^-) to dinitrogen (N_2) through a series of obligate intermediates including nitrous oxide (N_2O).[1−3] N_2O is an important greenhouse gas and ozone-depleting substance, so there is broad interest in limiting N_2O emissions from incomplete denitrification so as to minimize tradeoffs between improved water quality and inadvertent greenhouse gas (GHG) emissions.[4−7] The production, consumption, and emission of N_2O from subsurface porous media environments is described by the conceptual "hole-in-the-pipe" model, in which N_2O "leaks" out from "holes" in the denitrification process pipe.[8] Understanding of the complex processes that regulate the holes in the denitrification process pipe, particularly the mechanisms of water−air gas transfer, remains incomplete.

Woodchip bioreactors (WBRs) are sustainable systems that promote denitrification at terrestrial−aquatic interfaces using lignocellulosic woodchips as slow-release sources of carbon and as the electron donor for denitrifying biofilms colonizing the woodchip surfaces.[9,10] WBRs effectively remove NO_3^- from nonpoint sources including agricultural drainage, storm-water runoff, and septic system effluent,[10−13] and the U.S. Department of Agriculture issued a National Conservation Practice standard for denitrifying bioreactors in 2015. Although the complex processes controlling spatiotemporal variability in N_2O emissions from WBRs and other environments are a topic of major research interest,[1,14] the contribution of physical gas transport processes and water−air mass transfer to variability in N_2O emissions have received relatively little attention.[15−17]

An important physical control on dissolved gas behavior in porous media is the presence of gas-filled voids within otherwise water-saturated media.[17−20] Sparingly soluble dissolved gases partition into these trapped gas phases, retarding their transport through porous media.[18,21−23] While these partitioning processes have to our knowledge been studied in the context of N_2O, the environmental implications of these processes may be significant because they remove biologically active gases from microbial activity and may lead to "hot moments" of trace gas fluxes when water levels drop and trapped gases are liberated. Capillary trapping of residual gas phases in porous media during imbibition is a function of the pore size distribution,[22] with smaller pore sizes associated with greater entrapped gas volumes.[20] The overall porosity of WBRs ranges from 0.7 to 0.9 and consists of an interporosity

Received: August 9, 2019
Revised: November 8, 2019
Accepted: November 18, 2019
Published: November 18, 2019

DOI: 10.1021/acs.est.9b04829
Environ. Sci. Technol. 2019, 53, 14348−14356

(i.e., the pore space between woodchips) of ~0.5−0.6 and an intraporosity (i.e., pore spaces inside wood media) of 0.2−0.45.[9,24,25] The pore radii of wood media range from 50 nm to 500 μm, depending on the tree species.[26] The intrapore structure of woodchips may act as an important reservoir of trapped gas phases in otherwise saturated WBRs because of the small diameter of the pores.

The objective of this study was to explore the effects of gas-filled void volumes on the fate and transport of dissolved gases, particularly the biogenic GHGs N_2O and methane (CH_4), in otherwise water-saturated WBRs. We hypothesize that rising water levels lead to entrapment of gas phases inside WBRs, either in the interporosity between woodchips or in the intrapore structure within woodchips. Partitioning into gas-filled voids removes gases from microbial activity and can trigger episodic high flux events when water levels fall, and trapped gas phases are reconnected to the unsaturated zone. Dissolved gas tracer experiments in a laboratory model WBR were interpreted using an advection-dispersion mass transfer model to quantify the volume of gas-filled voids and first-order rate coefficients for mass transfer into trapped gas phases. Model parameters determined using biologically inactive tracers were used to simulate effects of bubble partitioning on transport of N_2O and CH_4 and thereby separate the effects of microbial consumption from mass transfer into gas-filled voids. Complementary modeling and measurement of the recovery of N_2O and CH_4 in the reactor headspace (HS) during water table drawdowns was used to evaluate the significance of these partitioning processes for episodic GHG fluxes. While this research focuses on processes in WBRs, insights gained here will be discussed in the broader context of biogenic GHG transport through porous media environments subject to hydrological variability.

2. MATERIALS AND METHODS

2.1. Model Framework. Small volumes of gas-filled void space in otherwise water-saturated media can retard the transport of, and consequently serve as a reservoir for, sparingly soluble trace gases.[19,21] Prior research has demonstrated the need for kinetically limited advection−dispersion-mass transfer models to effectively describe dissolved gas transport through porous media with trapped gas phases.[18,27] Assuming the presence of a single dissolved gas component and a constant gas phase volume, one-dimensional non-equilibrium gas transport in the presence of gas-filled voids can be described with a mobile−immobile interphase mass transfer kinetic model,[18] where the mobile phase describes the aqueous component, and the entrapped gas phase represents the immobile phase

$$\frac{\partial c_m}{\partial t} + \frac{V_g}{V_w}\frac{\partial c_g}{\partial t} = D\frac{\partial^2 c_m}{\partial x^2} - v\frac{\partial c_m}{\partial x} \quad (1)$$

D is the dispersion coefficient [$L^2\ T^{-1}$], v is the mean porewater velocity [$L\ T^{-1}$], c_m is the solute concentration in the mobile water phase [$M\ L^{-3}$], and V_g/V_w is the ratio of gas-filled to water-filled pore volume [dimensionless]. c_g is the concentration of gas in the immobile gas phase [$M\ L^{-3}$], and

$$\frac{\partial c_g}{\partial t} = \alpha(Hc_w - c_g) \quad (2)$$

H is the dimensionless air−water partition coefficient, and α is a first-order mass transfer rate coefficient [T^{-1}]. That, in this case, describes the diffusion-limited transfer of gas between the mobile water phase to the trapped gas phase. Equation 1 can be reduced to a dimensionless form (eq S5) used in analytical model solutions.[28]

Studies of nitrate reactive transport through WBRs have found that roughly 25−33% of the water in WBRs is held as a stagnant water volume within woodchips.[9,29,30] Gas-filled void spaces may be in either the mobile domain (i.e., the interporosity) or stagnant domain (i.e., the intrapore structure). In order to describe solute exchange between mobile and stagnant domains, as well as gas partitioning into trapped gas phases in both domains, we also implement a dual porosity model[31]

$$\theta_m\frac{\partial c_m}{\partial t} + \frac{V_{g,m}}{V_{w,m}}\frac{\partial c_{g,m}}{\partial t} + \theta_{im}\frac{\partial c_{im}}{\partial t} + \frac{V_{g,im}}{V_{w,im}}\frac{\partial c_{g,im}}{\partial t} = \theta_m D\frac{\partial^2 c_m}{\partial x^2} - \theta_m v\frac{\partial c_m}{\partial x} \quad (3)$$

θ_m and θ_{im} are the porosities of the mobile and stagnant domains, respectively. c_m and c_{im} are solute concentrations in the mobile and stagnant water phases, respectively, while $c_{g,m}$ and $c_{g,im}$ are the gas concentrations in gas-filled voids in the mobile and stagnant domains, respectively. $V_{g,m}/V_{w,m}$ and $V_{g,im}/V_{w,im}$ are the ratio of gas-filled to water-filled void space in the mobile and stagnant domains, respectively. Equation 3 can also be rewritten in dimensionless form and implemented using analytical solutions.[28] The dimensionless form of eqs 1 and 3 (eq S5) includes the retardation factor R,

$$R = 1 + H\frac{V_g}{V_w} \quad (4)$$

V_g/V_w is a physical property of the reactor and is therefore independent of the gas, while R values are a function of H and therefore vary with different gases (see Table S1 for H values of gases examined in this study). A complete description of the nonequilibrium model, including detailed description of the dimensionless variables, is in the Supporting Information. Models are parameterized using dissolved gas tracer tests in a laboratory WBR.

2.2. Reactor Design. A laboratory reactor (30 cm × 20 cm h × 5 cm w) was constructed using a poly(vinyl chloride) frame and transparent polycarbonate siding with four inlet and four outlet ports at the ends of the reactor to achieve quasi one-dimensional flow through the reactor (Figures S1−S3). The reactor face was fitted with a planar optode (PreSens GmbH, Regensburg, Germany) for dissolved oxygen (DO) monitoring. The upper 7.5 cm of the reactor was separated into three HS compartments fitted with butyl stoppers for HS gas sampling.

Ash (genus Fraxinus) woodchips were obtained from a lumber mill in Cayuta, NY and sorted to a maximum size of 2.5 cm × 2.5 cm × 1 cm. Woodchips were conditioned in a flow-through reactor with 0.32 mM NO_3^- for 9 months at a hydraulic residence time of 24 h to promote denitrifying biofilm formation on woodchips. The total porosity of the bioreactor was determined through the summation of the drainable porosity and the specific retention.[9] The drainable porosity, equivalent to the interporosity, (θ_m) was calculated as the volume of water drained from the reactor divided by the total woodchip-packed reactor volume. The specific retention, equivalent to the intraporosity, (θ_{im}) was determined using the

DOI: 10.1021/acs.est.9b04829
Environ.Sci.Technol.2019,53, 14348−14356

mass difference between wet and dry woodchips after 48 h at 105 °C.[9]

2.3. Dissolved Gas Tracer Tests. Tracer tests with dissolved gases as partitioning tracers were performed to estimate the volume of trapped gas phases in the bioreactor as a function of antecedent hydraulic conditions, through the parameterization of gas transport models. Recovery of gases in the reactor HS after reactor drainage was used to evaluate the contribution of gas partitioning into trapped gas phases to flux events following water-level drawdowns. Abiotic experiments were performed by inhibiting microbial activity with 50 mM sodium azide,[32] with the purpose of quantifying the effects of gas transfer processes on tracer mass balances without confounding microbial influences. Antecedent hydraulic conditions in the reactor were classified as "transient" or "static" (Table 1). Transient conditions involved reactor drainage 36 h prior to the experimental start, and then a water table rise of 12 cm/h immediately prior to the experimental start. Static conditions were characterized by a slower water table rise of 1.7 cm/h at least 12 h prior to the experimental start, with no flow until the tracer injection.

Table 1. Experimental Descriptions

media	hydrology	water table rise rate (cm/h)	additional description
glass beads	transient	12.0	drained 36 h prior to experiment
abiotic woodchips	static	1.65	pore space flushed with CO_2 prior to experiment
	transient	12.0	drained 36 h prior to experiment
biotic woodchips	transient	12.0	drained 36 h prior to experiment

Tracer tests with three levels of complexity were performed. The first and simplest case involved a set of abiotic, transient experiments in 1 mm glass bead media. These experiments probed entrapment of gas-filled voids in a uniform media and permitted comparison of gas tracer-based V_g/V_w estimates to existing measurements of trapped gas volumes via X-ray microtomography.[20] Second, transient and static abiotic experiments were performed in a woodchip-filled reactor. These experiments quantified gas entrapment in WBRs as a function of antecedent conditions and allowed for the validation of techniques for simulating transport of N_2O and CH_4 based on parameters estimated from conservative gas tracers. The third set of experiments ("biotic" experiments) was conducted in microbially active woodchip media and was used to separate the contribution of microbial consumption/production of gases from partitioning into trapped gas-filled voids as sinks for CH_4 and N_2O in WBRs. Experimental conditions are summarized in Table 1. All conditions were tested in duplicate.

Step input gas tracer tests were performed by injecting a tracer solution into the four inlet ports using a peristaltic pump to achieve steady-state flow with a calculated hydraulic retention time of 1.75 h. The tracer solution contained dissolved N_2O, CH_4, C_2H_6, He, and SF_6 as gas tracers and bromide (Br^-) as a nonvolatile, nonsorbing tracer (Table S1). At the end of the experiments, the water table was lowered by draining the reactor over a period of approximately 20 min. Experiments were conducted at 24 °C in a temperature-controlled room.

2.4. Sampling and Chemical Analysis. Effluent samples were collected to develop tracer breakthrough curves. Water samples were collected with glass syringes, transferred to crimp-sealed vials, and analyzed via gas chromatography (GC) (Shimadzu GC-2014 with AOC-5000 autosampler). Water from the GC vials was analyzed for Br^- on an ion chromatograph (Thermo ICS-2100).

HS gas samples were collected using plastic gas-tight syringes by injecting a known volume of N_2 into the sealed HS through butyl septa, mixing the HS via syringe pumping, and withdrawing the same volume of HS gas for GC analysis. HS samples were collected during steady-state flow and for 3 h after the reactor drainage.

2.5. Curve Fitting and Parameter Estimation. Analytical solutions[28] for nonequilibrium transport models (eqs S3 and S8) were implemented in MATLAB to fit breakthrough curves in order to estimate reactor hydrodynamic properties (v; D) and gas exchange parameters (V_g/V_w; α). The mobile−immobile interphase mass transfer kinetic model was used to fit breakthrough curves in the glass bead media,[18,33] while the dual porosity model was used to model transport through the woodchip media because of the significant volume of the stagnant water domain in the internal woodchip pores.[30] $\varphi_{m,}$ the mobile aqueous fraction, was fixed based on measurements of θ_m and θ_{im} (see Section 2.2) and calculated as $\theta_m/(\theta_m + \theta_{im})$. Bromide curves were used to estimate v and D by minimizing the sum of squared residuals (SSR) between the data and model fit. With v and D fixed, dissolved gas tracer curves were fit by systematically iterating through values of α, R, and R_m and identifying the parameter set that minimized the SSR. R and R_m are the overall retardation factor because of bubble partitioning and the retardation factor because of bubble partitioning in the mobile domain, respectively. Values of R and R_m were utilized to determine V_g/V_w and $V_{g,m}/V_{w,m}$ using eqs 4 or S10 and H for each gas (Table S1).

In biotic experiments, overall V_g/V_w values were taken as the average of the V_g/V_w values estimated from the three conservative gas tracers (SF_6, He, and C_2H_6). $V_{g,m}/V_{w,m}$ values determined with C_2H_6 and SF_6 were averaged to obtain an estimate of $V_{g,m}/V_{w,m}$ for nonconservative tracer gases. Helium was excluded from this average $V_{g,m}/V_{w,m}$ as its diffusion coefficient significantly varies from the diffusivities of C_2H_6 and CH_4. Gas-specific α values were taken as an average of α from replicate abiotic experiments subjected to identical antecedent hydrologic conditions. The suitability of this approach for modeling breakthrough curves was evaluated by using He and SF_6 breakthrough curves for model parameterization and then testing the simulated C_2H_6 breakthrough curve against measured C_2H_6 data. Helium and SF_6 data from transient biotic experiments were used to estimate overall V_g/V_w. In the case of $V_{g,m}/V_{w,m}$, the parameter obtained for SF_6 was used as the estimate for C_2H_6. C_2H_6 data from transient abiotic experiments were used to estimate α. The simulated C_2H_6 curve was in good agreement with C_2H_6 measurements (Figure S4).

2.6. X-ray-Computed Microtomography. High-resolution X-ray-computed microtomography (μCT) was used to probe the internal pore structure of woodchip media and quantify ratios of water-filled to gas-filled void space in the woodchip intraporosity. Xradia Zeiss VersaXRM-520 was used to capture three-dimensional images of dry woodchips and woodchips that had been immersed in a 3% iodine solution for either 8 h or one week. The dimensions of the scanned

DOI: 10.1021/acs.est.9b04829
Environ.Sci.Technol.2019,53, 14348−14356

woodchips were approximately 3.5 × 2 × 5 mm, and iodine was used to enhance phase contrast between the solution and wood material. Projections were reconstructed to three-dimensional volumes using Avizo Lite (version 9.7.0). Phase segmentation was used to quantify ratios of gas-filled to water-filled pore space by classifying voxels as air-filled pores, iodine-filled pores, wood, or bulk iodine solution, using voxel (3-dimensional pixel) intensities in Avizo Lite.

3. RESULTS

3.1. Tracer Breakthrough Curves in Abiotic Conditions. Tracer breakthrough curves in transient glass bead, static woodchip, and transient woodchip experiments indicate that dissolved gas breakthrough was retarded relative to the bromide tracer because of partitioning into gas-filled voids (Figure 1) (Table 2). Gases eluted in the order N_2O, CH_4, C_2H_6, SF_6, and He in the glass bead experiments, while in woodchip experiments, gases eluted in the order N_2O, SF_6, CH_4, C_2H_6, and He. Gas tracers were retarded to a greater extent in the transient woodchip case (Figure 1C) compared to the transient glass bead and static woodchip cases (Figure 1A,B). In transient glass bead and static woodchip cases, N_2O breakthrough curve is nearly concurrent with bromide, while in the transient woodchip case, N_2O and bromide breakthrough curves are clearly separated. Although SF_6 has the greatest H value and would experience the greatest retardation under equilibrium conditions (eq 4), helium demonstrated the greatest retardation.

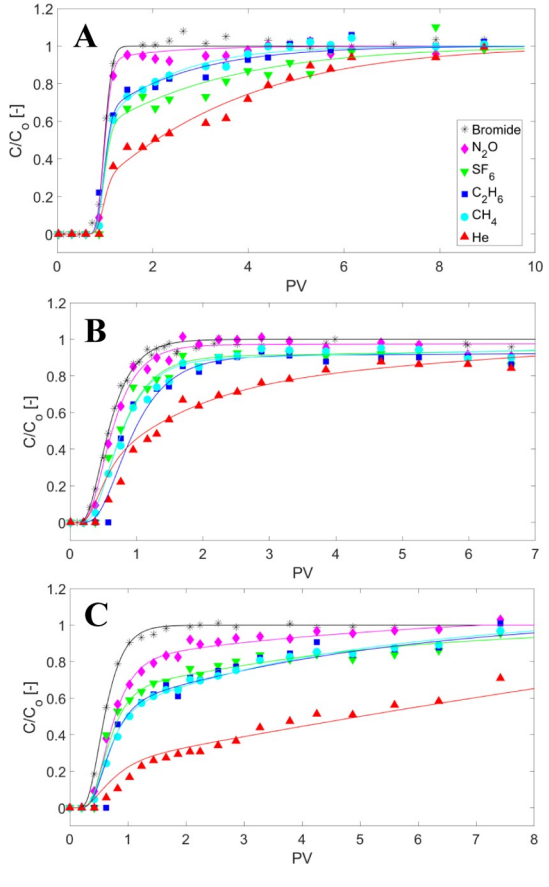

Figure 1. Bromide and dissolved gas concentrations in the reactor effluent (symbols) and model fits (lines) for (A) a glass bead-packed reactor; (B) an abiotic woodchip reactor with a static water table; and (C) an abiotic woodchip reactor with a transient water table. Model fits for (A) are generated using a mobile−immobile interphase mass transfer kinetic model, and fits in (B,C) are generated using the dual porosity nonequilibrium model. Duplicate experiments in the Supporting Information.

Table 2. Duplicate Experiment Physical Parameters

experiment	v ×10^{-5} (m/s)	D × 10^{-6} (m^2/s)	peclet #
glass beads 1	7.45	0.18	413.9
glass beads 2	7.67	0.22	348.6
abiotic,static 1	7.13	2.75	25.91
abiotic,static 2	6.40	3.80	16.84
abiotic,transient 1	7.88	2.19	36.00
abiotic,transient 2	7.06	4.81	14.67
biotic, transient 1	3.63	1.03	35.37
biotic, transient 2	3.84	1.01	38.18

3.2. Model Parameters. From measured θ_m and θ_{im} values of 0.59 and 0.31, respectively, φ_m was calculated as 0.65, similar to previously reported values.[9,29,30] Although there was some variation in V_g/V_w estimated by different gases in each experimental condition, there was overall good agreement for V_g/V_w. Consistent with visual observations of negligible bubble entrapment in the reactor interporosity, $V_{g,m}/V_{w,m}$ values were an order of magnitude lower than overall V_g/V_w values (Table S3), suggesting that most gas-filled voids were located in the woodchip intraporosity and not in the interporosity. Transient woodchip V_g/V_w estimates ranged from 0.15 to 0.28 and were approximately twice the values in static woodchip experiments and an order of magnitude larger than those in glass bead experiments (Tables S2 and S3).

3.3. Mass Balances of Gases in Reactor Compartments Inferred from Breakthrough Curve Analysis. Mass balances of N_2O and CH_4 in abiotic static and transient experiments were generated based on breakthrough curve analysis (Figure 3) with underlying calculations available in the Supporting Information. In static woodchip experiments, 97−98% of injected N_2O and 86−89% of injected CH_4 are exported from the reactor dissolved in the effluent. In transient experiments, these values decrease to approximately 92 and 80−81% for N_2O and CH_4, respectively. The balance of the N_2O and CH_4 masses was retained inside the reactor, presumably in gas-filled voids. This approach does not allow for disaggregation of the reactor-retained mass into specific reactor compartments (i.e., flux to the reactor HS during steady-state flow conditions vs partitioning into trapped gas-filled voids in the otherwise water-saturated zone).

3.4. Mass Balances of Gases in Reactor Compartments through Direct HS Measurements. Direct measurements of gas concentrations in the reactor HS before and after the water table drawdown were used to determine the role of different reactor compartments in gas retention. Gas concentrations in the HS before the water table drawdown were used to quantify the contribution of diffusive water−air flux during steady-state flow. Fluxes to the HS during and after the water level drawdown were assumed to represent gas that had partitioned into gas-filled voids trapped below the water level, which was then released when voids were reconnected to the HS by the water table drawdown. The allocation of reactor-retained gases into the HS and trapped gas-filled voids is summarized in Figure 3 (right bar of each condition). The tracer mass exported in the effluent was estimated from the breakthrough curve analysis.

DOI: 10.1021/acs.est.9b04829
Environ.Sci.Technol.2019,53, 14348−14356

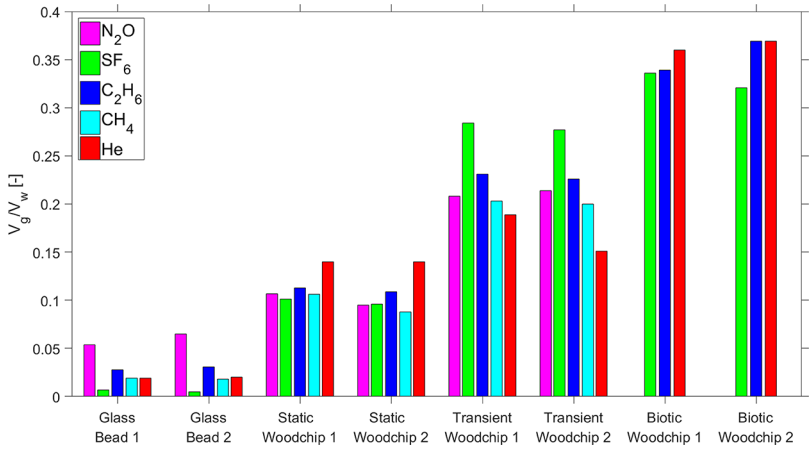

Figure 2. Overall V_g/V_w estimated with dissolved gas tracer experiments in different media and antecedent hydrological conditions. The bar color indicates the V_g/V_w estimation determined for each gas. Numbering indicates replicate experiments.

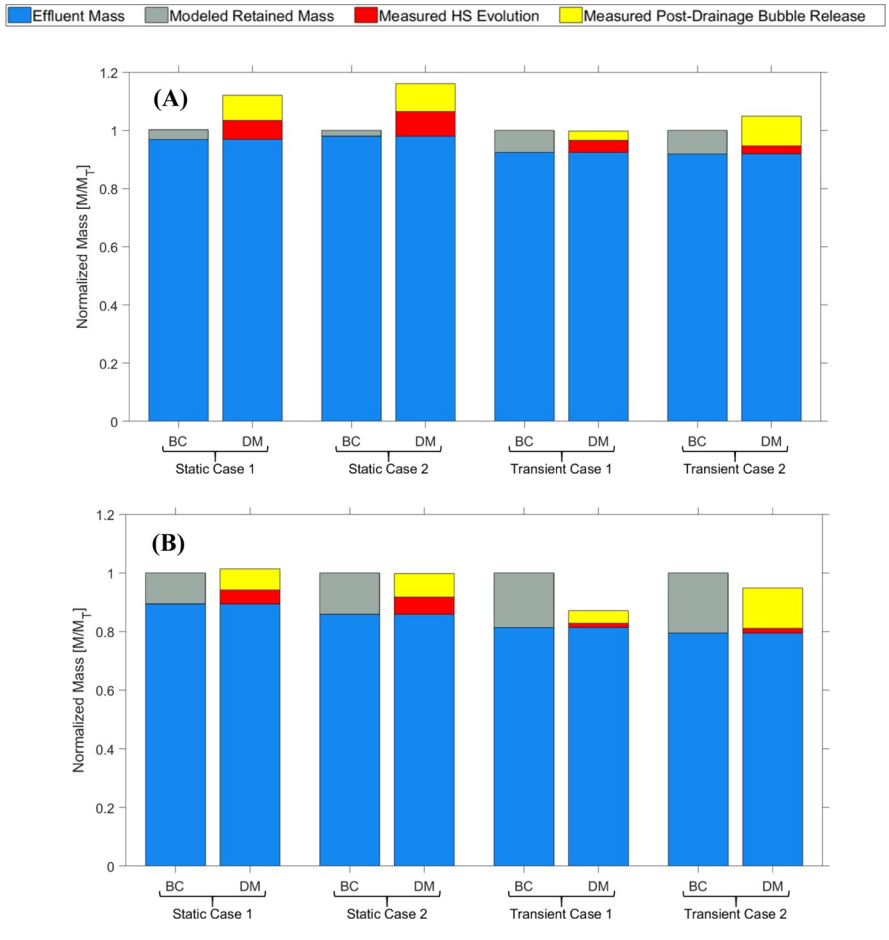

Figure 3. Mass balances of N_2O (A) and CH_4 (B) in abiotic static and transient experiments. Masses are normalized to the total mass (M_T) injected into the reactor. For each case, the left bar shows the mass balance inferred from breakthrough curve analysis, and the right bar represents the mass balance based on headspace (HS) measurement before and after reactor drainage. Blue shading indicates effluent mass, gray shading indicates retention in the reactor, red shading indicates mass in the HS before drainage, and yellow shading indicates mass released during reactor drainage. Numbering indicates replicate experiments.

In static cases, gas transfer to the HS prior to the water table drawdown represents 6.5−8.4 and 4.6−5.9% of the injected N_2O and CH_4 mass, respectively. For transient cases, these values decrease to 2.9−4.1% for N_2O and 1.5−1.6% for CH_4. Partitioning into gas-filled voids accounts for 8.7−9.7% of N_2O and 7.2−7.9% of CH_4 mass in static cases. These values are 3.3−10 and 4.3−14% for N_2O and CH_4, respectively, in transient cases. Estimates of retained mass based on effluent breakthrough curves (gray components of stacked bars) were generally consistent with gas recovery in the reactor HS (sum of the yellow and red components of stacked bars). Estimates of retained N_2O based on breakthrough curves typically

DOI: 10.1021/acs.est.9b04829
Environ.Sci.Technol.2019,53, 14348−14356

underestimated the mass of N_2O recovered by up to 16%, while breakthrough curve-based estimates for CH_4 typically overestimated the mass recovered up to 13%. After reactor drainage, gas masses in the reactor HS stabilized faster in the glass bead case than in the woodchip cases (Figures S11 and S12).

3.5. Tracer Breakthrough Curves in Biotic Conditions. Comparison of simulated N_2O and CH_4 breakthrough curves with observed N_2O and CH_4 breakthrough curves allows for the contribution of microbial N_2O and CH_4 production/consumption to be separated from gas partitioning into trapped gas-filled voids as trace gas sinks (Figure 4). The

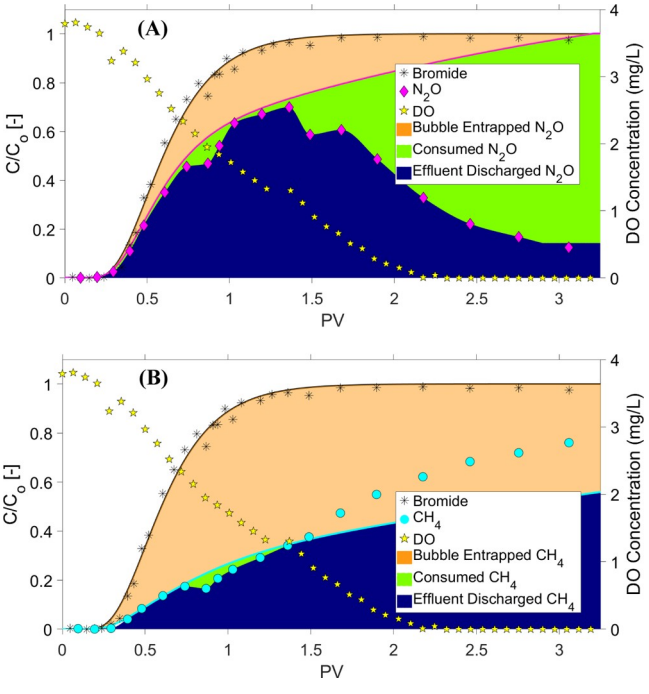

Figure 4. Effluent concentrations of N_2O (A) and CH_4 (B) in the effluent from biotic experiment measurements (symbols) and models based on gas partitioning (solid lines). DO concentrations (stars) were measured with the planar optode and indicate the average concentration in the final third of the reactor. Blue shading represents mass released from the system in the effluent. Green shading in (A) represents mass consumed by microbial activity. Beige shading indicates mass partitioned into trapped gas-filled voids.

measured N_2O curve accounted for 51% of the total effluent mass estimated by the simulated N_2O breakthrough curve. The divergence of these curves, beginning when DO concentrations were ~1 mg/L, illustrates the effect of microbial N_2O reduction on the hypoxic reactor. For CH_4, measured mass was 25% greater than effluent mass estimated by the simulated CH_4 breakthrough curve, indicating a microbial source of CH_4.

3.6. Estimates of Woodchip Intraporosity and V_g/V_t with µCT. µCT was used to probe the interpore structure of woodchips immersed in 3% iodine solution for either 8 h or one week (Figure 5). Phase segmentation analysis quantified the gas-filled pore volume inside woodchips (V_g) normalized by the total woodchip volume (V_t). V_g/V_t was approximately 0.32 for a woodchip that had been immersed in solution for 8 h and decreased to 0.09 for a woodchip that had been immersed in solution for one week. Analysis of a dry woodchip yielded a V_g/V_t value of 0.75, at the upper end of previously reported wood porosities.[26]

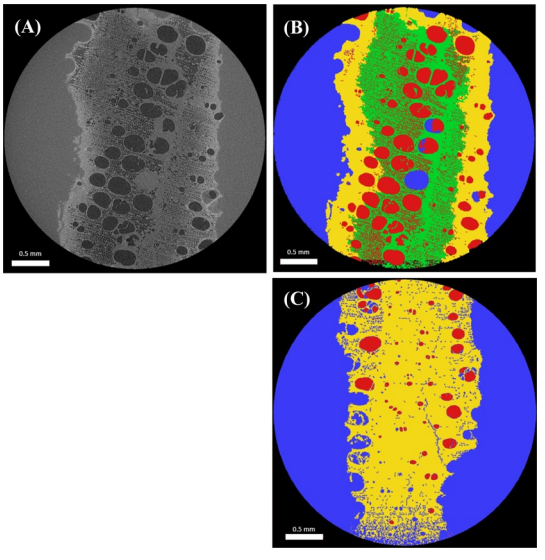

Figure 5. µCT images of woodchips soaked in 3% iodine solution for 8 h (A,B) and one week (C). (A) Shows the original image, and (B) shows the false color image generated by phase segmentation. In false color images (B,C), blue is the iodine solution, red is the gas-filled voids, yellow is the wet woodchip, and green is the dry woodchip.

V_g/V_w estimates from transient tracer experiments coupled with measurements of reactor θ_m and θ_{im}, correspond to woodchip V_g/V_t values during experiments of 0.34−0.57 (detailed calculations are available in Supporting Information). Although the V_g/V_t values inferred from gas tracer experiments differ somewhat from the value determined with µCT, they both support the interpretation that a significant fraction of the woodchip intraporosity is gas-filled after approximately 8 h of immersion in water.

4. DISCUSSION

4.1. Partitioning into Gas-Filled Voids in Glass Bead Media. Transport of dissolved gases through the glass bead-packed reactor was retarded relative to the nonvolatile bromide tracer because of the transfer of gases from the mobile water phase to trapped gas phases (Figure 4). Fitting the mobile−immobile interphase mass transfer kinetic model to breakthrough curves yielded V_g/V_w estimates of 0.01−0.07, similar to findings in Mohammadian et al. (2015), who used µCT to determine V_g/V_w values of 0.026−0.064 in a 1 mm glass bead media.[20] Geistlinger et al. reported V_g/V_w ratios of 0.013−0.027 in glass bead media based on µCT analysis.[22] Kava et al. (2002) used SF_6 and krypton in a gas tracer approach to estimate bubble entrapment in sand columns. They found α values for SF_6 of 9.31×10^{-5} to 7.19×10^{-4} s^{-1} at pore velocities of 0.01−0.04 cm/h[18], similar to SF_6 α values determined here of 1.2×10^{-4} to 2.45×10^{-4} s^{-1} with a pore velocity of 0.007 cm/h. While these and other studies[19,21,33,34] have explored the role of residual gas-filled voids in partitioning of inert tracers or oxygen, the present study is the first to our knowledge to address the effects of partitioning processes for the transport of N_2O and CH_4 and explore the implications for episodic fluxes when water levels fluctuate. Assumptions about a single dissolved gas component and a constant gas phase volume may not necessarily hold true in these experimental conditions. The use of multiple dissolved gas tracers leads to a multicomponent system, and mass transfer of these gases into entrapped bubbles with concurrent

DOI: 10.1021/acs.est.9b04829
Environ.Sci.Technol.2019,53, 14348−14356

dissolution of entrapped oxygen into the mobile aqueous phase could lead to a variable gas phase volume. Although the simpler modeling approach employed here appropriately describes measured breakthrough curves and has previously been applied to similar multicomponent systems,[27] there may be detailed features of the data that are better described by a multicomponent model that accounts for variable gas volumes.[35]

4.2. Partitioning into Gas-Filled Voids in WBRs: Significance of Woodchip Intraporosity. Both static and transient conditions in the woodchip media led to greater entrapment of gas-filled voids than transient conditions in the glass bead media, indicating that there are characteristics of the woodchip media that are more conducive for gas entrapment. Transient hydrological conditions led to a larger trapped bubble volume (V_g/V_w from 0.19−0.28) than static conditions (V_g/V_w from 0.09−0.14). These values are higher than those reported for glass bead or sand media, although larger values of 0.28−0.41 have been observed in sandstone.[36]

Three lines of evidence point to entrapment of gas-filled voids in the woodchip intraporestructure as the primary reservoir of trapped gas phases. First, visual inspection of the woodchip media through the reactor transparent face during tracer experiments showed the negligible presence of bubbles. Second, parameters estimated from tracer data showed that V_g/V_w in the mobile domain (i.e., $V_{g,m}/V_{w,m}$) was very small relative to overall V_g/V_w, indicating a significant volume of trapped gas volume in the stagnant domain (i.e., in the woodchip internal porosity) (Table S3). Finally, μCT confirmed that a significant fraction of the woodchip intraporosity remains gas-filled after 8 h (Figure 5). V_g/V_w values determined by inert gas tracers were even higher under transient microbially active conditions, reaching values of 0.33−0.36 which correspond to 24% of the bioreactor pore volume being occupied by trapped gas phases (Figure 2). Although the reasons for this are not clear, one plausible explanation is that biogenic gas formation increased the volume of trapped gas phases.

A key distinction between the glass bead and woodchip media is that the woodchips trap a larger volume of gas-filled voids (Figure 2), and these trapped gas phases are primarily located in the reactor intraporosity (i.e., internal woodchip pore structure). This has implications for the magnitude and timing of trace gas flux to the atmosphere when water tables fall. For example, fluxes of N_2O and CH_4 to the reactor HS after bioreactor drainage were greater in woodchip than glass bead experiments because of greater trapping of gas-filled voids and partitioning of dissolved gases into these voids (Figures S11 and S12). Moreover, HS masses of N_2O and CH_4 stabilize after approximately 75 min in glass bead experiments, while in woodchip experiments, masses continue to increase through 150 min. The time lag between drainage and flux to HS in woodchip experiments could be because of rate-limited transfer out of the woodchip intraporosity, while in the glass bead media gases were released to the HS as soon as the falling water table reconnected bubbles trapped in the interporosity with the reactor HS.

4.3. Separating Effects of Gas Partitioning from Microbial Consumption/Production on N_2O and CH_4 Dynamics. In biotic woodchip experiments, parameters estimated from breakthrough curves of inert tracers were used to simulate N_2O and CH_4 behavior controlled by physical−chemical processes (e.g., advection, dispersion, and bubble partitioning) without the influence of microbial activity. Comparison of simulated breakthrough curves with measured N_2O and CH_4 curves provides insights into the contribution of physical−chemical versus microbial processes in controlling the fate of N_2O and CH_4. Microbial consumption is the largest N_2O sink in the reactor, with the rates of N_2O consumption accelerating at approximately 1.5 PV, corresponding to DO ≤ 1 mg/L (Figure 4a). 1 mg/L is the approximate DO threshold below which microbial N_2O reduction is initiated in pure culture studies.[37] Although the microbial N_2O sink is important once the reactor is hypoxic, we estimate that in biotic experiments, 16% of injected N_2O partitions into gas phases and is unavailable for microbial consumption. This may overestimate the true extent of N_2O partitioning because it is based on the transport of an inert gas, while in microbially active media, some N_2O will be consumed before contacting gas-filled voids. Nonetheless, this finding highlights the fact that in media with trapped gas-filled voids, a portion of the N_2O in the system will be retained in a biologically unavailable form as long as the dissolved N_2O concentration is constant. If dissolved N_2O concentrations decrease, the trapped gas-filled voids will be a source of N_2O transfer back into the water phase.

Partitioning of CH_4 into trapped gas phases is more significant than partitioning of N_2O, due to the larger H for CH_4. Approximately 58% of the injected CH_4 is estimated to partition into trapped gas-filled voids in biotic woodchip experiments. The divergence between simulated and measured CH_4 curves increases after 1.5 PVs, corresponding to the transition to hypoxic conditions and consistent with net CH_4 production occurring under hypoxic to anoxic conditions. The estimate of CH_4 in trapped gas-filled voids may be an underestimate because dissolved CH_4 concentrations in contact with bubbles are greater than those predicted by inert tracers.

4.4. Environmental Implications. Drying−rewetting cycles in a laboratory WBR lead to greater entrapment of gas-filled voids within the bioreactor compared to a static water level. Recent research has suggested that drying−rewetting cycles increase nitrate removal rates in WBRs,[38] and the USDA's Conservation Practice Standard for denitrifying bioreactors recommends draining bioreactors during no-flow conditions.[39] The findings presented here suggest that hydraulic management of WBRs involving dry−wet cycles will enhance entrapment of trapped gas phases, primarily in the woodchip intraporosity. Dissolved gases in the bioreactor influent, or produced via microbial activity in the bioreactor, will partition into these trapped gas phases. In the case of N_2O, partitioning into gas-filled voids makes N_2O unavailable for N_2O-reducing microbes and can reduce the extent of microbial N_2O reduction in the reactor. These partitioning processes will also lead to episodic fluxes of N_2O and CH_4 emissions when water levels fall because N_2O and CH_4 that had partitioned into trapped gas phases will be released when trapped bubbles are liberated. The role of these bubble-mediated "hot moments"[40] of GHG flux will likely be more significant for CH_4 than for N_2O because CH_4 partitions into bubbles to a greater extent than N_2O because of its higher H value. Although the significance of bubble-mediated fluxes, or ebullition, of CH_4 from wetlands and aquatic sediments are well-known,[41,42] the role of bubble-mediated N_2O fluxes has received less attention. Although some studies have found that bubble-mediated fluxes play a minor role in N_2O emissions

DOI: 10.1021/acs.est.9b04829
Environ.Sci.Technol.2019,53, 14348−14356

from streams,[43] the present study shows that a falling water table triggered a release of N_2O accounting for up to 10% of the total mass of N_2O injected into the WBR, and that this bubble-mediated flux was more important than diffusive flux across the water−air interface. This study demonstrates that N_2O transfer from water into gas-filled voids in otherwise water-saturated media may be an important, though largely overlooked, control on N_2O transport and fate in denitrifying subsurface environments.

There are a number of environmental variables and design considerations beyond hydraulic management that may influence trapping of residual gas phases and their impact on fate and transport of dissolved gases in WBRs. For example, there is growing interest in the performance of WBRs and other passive biofiltration systems in cold weather conditions.[44,45] Although the greatest impact of low temperatures is expected to involve rates of microbial activity, partitioning of biogenic gases into trapped bubbles will likely decrease because of the greater water solubility of N_2O and CH_4 at low temperatures.[46] A notable modification to WBR design with potential relevance for gas-trapping processes is the amendment of biochar to bioreactor media to enhance removal of nutrients and trace organic pollutants.[47−49] Biochar is characterized by a high porosity,[50] and an increase in the internal pore volume of bioreactor media will likely increase retention of residual gas phases, particularly if pore throats are narrow. Recent observations of entrapment of N_2O in a biochar-amended soil[16] may potentially be explained by gas partitioning between soil water and trapped gas phases in the biochar pore structure. There is also evidence that the intraporosity of woodchip media increases with age.[51] This could increase trapping of residual gas phases inside WBRs and, consequently, the episodic flux of N_2O when water levels within bioreactors fall.

ASSOCIATED CONTENT

* Supporting Information

The Supporting Information is available free of charge at https://pubs.acs.org/doi/10.1021/acs.est.9b04829.

Additional details on model development and data and experimental details (PDF)

AUTHOR INFORMATION

Corresponding Author

*E-mail: mcr239@cornell.edu.

ORCID

Matthew C Reid: 0000-0001-5185-7678

Notes

The authors declare no competing financial interest.

ACKNOWLEDGMENTS

Funding was provided by the NSF grant CBET-1804975 and the Cornell University Program in Cross-Scale Biogeochemistry and Climate, supported by the NSF-IGERT grant 1069193 and the Atkinson Center for a Sustainable Future. The authors thank P. Diamessis for discussions about model implementation, P. Charles for assistance in reactor construction, and T. Porri for assistance with μCT (NIH S10OD012287). Complete MATLAB scripts for transport models are available at https://github.com/ReidLab/nonequilibrium-nitrous.

REFERENCES

(1) Schlesinger, W. H. On the Fate of Anthropogenic Nitrogen. Proc. Natl. Acad. Sci. U.S.A. 2009, 106, 203−208.

(2) Mitsch, W. J.; Day, J. W.; Wendel Gilliam, J.; Groffman, P. M.; Hey, D. L.; Randall, G. W.; Wang, N. Reducing Nitrogen Loading to the Gulf of Mexico from the Mississippi River Basin: Strategies to Counter a Persistent Ecological Problem. Bioscience 2001, 51, 373.

(3) Freeman, C.; Lock, M. A.; Hughes, S.; Reynolds, B.; Hudson, J. A. Nitrous Oxide Emissions and the Use of Wetlands for Water Quality Amelioration. Environ. Sci. Technol. 1997, 31, 2438−2440.

(4) Wang, S.; Wang, W.; Liu, L.; Zhuang, L.; Zhao, S.; Su, Y.; Li, Y.; Wang, M.; Wang, C.; Xu, L.; et al. Microbial Nitrogen Cycle Hotspots in the Plant-Bed/Ditch System of a Constructed Wetland with N_2O Mitigation: Our Understanding of These Processes Has Significantly Changed. Environ. Sci. Technol. 2018, 52, 6226.

(5) Payne, E. G. I.; Pham, T.; Cook, P. L. M.; Deletic, A.; Hatt, B. E.; Fletcher, T. D. Inside Story of Gas Processes within Stormwater Biofilters: Does Greenhouse Gas Production Tarnish the Benefits of Nitrogen Removal? Environ. Sci. Technol. 2017, 51, 3703−3713.

(6) Quick, A. M.; Reeder, W. J.; Farrell, T. B.; Tonina, D.; Feris, K. P.; Benner, S. G. Controls on Nitrous Oxide Emissions from the Hyporheic Zones of Streams. Environ. Sci. Technol. 2016, 50, 11491−11500.

(7) Burgin, A. J.; Lazar, J. G.; Groffman, P. M.; Gold, A. J.; Kellogg, D. Q. Balancing Nitrogen Retention Ecosystem Services and Greenhouse Gas Disservices at the Landscape Scale. Ecol. Eng. 2013, 56, 26−35.

(8) Davidson, E. A.; Keller, M.; Erickson, H. E.; Verchot, L. V.; Veldkamp, E. Testing a Conceptual Model of Soil Emissions of Nitrous and Nitric Oxides. Bioscience 2000, 50, 667−680.

(9) Halaburka, B. J.; Lefevre, G. H.; Luthy, R. G. Evaluation of Mechanistic Models for Nitrate Removal in Woodchip Bioreactors. Environ. Sci. Technol. 2017, 51, 5156−5164.

(10) Lopez-Ponnada, E. V.; Lynn, T. J.; Peterson, M.; Ergas, S. J.; Mihelcic, J. R. Application of Denitrifying Wood Chip Bioreactors for Management of Residential Non-Point Sources of Nitrogen. J. Biol. Eng. 2017, 11−16.. DOI: 10.1186/s13036-017-0057-4

(11) Gorski, G.; Fisher, A. T.; Beganskas, S.; Weir, W. B.; Redford, K.; Schmidt, C.; Saltikov, C. Field and Laboratory Studies Linking Hydrologic, Geochemical, and Microbiological Processes and Enhanced Denitrification during Infiltration for Managed Recharge. Environ. Sci. Technol. 2019, 53, 9491−9501.

(12) Schipper, L. A.; Cameron, S. C.; Warneke, S. Nitrate Removal from Three Different Effluents Using Large-Scale Denitrification Beds. Ecol. Eng. 2010, 36, 1552−1557.

(13) Rambags, F.; Tanner, C. C.; Stott, R.; Schipper, L. A. Fecal Bacteria, Bacteriophage, and Nutrient Reductions in a Full-Scale Denitrifying Woodchip Bioreactor. J. Environ. Qual. 2016, 45, 847−854.

(14) Burgin, A. J.; Groffman, P. M. Soil O_2 Controls Denitrification Rates and N_2O Yield in a Riparian Wetland. J. Geophys. Res. 2012, 117, G01010.

(15) Firestone, M. K.; Davidson, E. A. Microbiological Basis of NO and N_2O Production and Consumption in Soil. Exchange of Trace Gases between Terrestrial Ecosystems and the Atmosphere; John Wiley & Sons, 1989.

(16) Harter, J.; Guzman-Bustamante, I.; Kuehfuss, S.; Ruser, R.; Well, R.; Spott, O.; Kappler, A.; Behrens, S. Gas Entrapment and Microbial N_2O Reduction Reduce N_2O Emissions from a Biochar-Amended Sandy Clay Loam Soil. Sci. Rep. 2016, 6, 39574.

(17) Geistlinger, H.; Jia, R.; Eisermann, D.; Florian Stange, C. Spatial and Temporal Variability of Dissolved Nitrous Oxide in Near-Surface Groundwater and Bubble-Mediated Mass Transfer to the Unsaturated Zone. J. Plant Nutr. Soil Sci. 2010, 173, 601−609.

(18) Vulava, V. M.; Perry, E. B.; Romanek, C. S.; Seaman, J. C. Dissolved Gases as Partitioning Tracers for Determination of Hydrogeological Parameters. Environ. Sci. Technol. 2002, 36, 254−262.

DOI: 10.1021/acs.est.9b04829
Environ. Sci. Technol. 2019, 53, 14348−14356

(19) Heilweil, V. M.; Kip Solomon, D.; Perkins, K. S.; Ellett, K. M. Gas-Partitioning Tracer Test to Quantify Trapped Gas during Recharge. Ground Water 2004, 42, 589−600.
(20) Mohammadian, S.; Geistlinger, H.; Vogel, H.-J. Quantification of Gas-Phase Trapping within the Capillary Fringe Using Computed Microtomography. Vadose Zone J. 2015, 14 5. DOI: 10.2136/vzj2014.06.0063
(21) Fry, V. A.; Istok, J. D.; Semprini, L.; O'Reilly, K. T.; Buscheck, T. E. Retardation of Dissolved Oxygen Due to a Trapped Gas Phase in Porous Media. Groundwater 1995, 33, 391.
(22) Geistlinger, H.; Mohammadian, S.; Schlueter, S.; Vogel, H.-J. Quantification of Capillary Trapping of Gas Clusters Using X-Ray Microtomography. Water Resour. Res. 2014, 50, 4514−4529.
(23) Holocher, J.; Peeters, F.; Aeschbach-Hertig, W.; Kinzelbach, W.; Kipfer, R. Kinetic Model of Gas Bubble Dissolution in Groundwater and Its Implications for the Dissolved Gas Composition. Environ. Sci. Technol. 2003, 37, 1337−1343.
(24) Pluer, W. T.; Geohring, L. D.; Steenhuis, T. S.; Walter, M. T. Controls Influencing the Treatment of Excess Agricultural Nitrate with Denitrifying Bioreactors. J. Environ. Qual. 2016, 45, 772−778.
(25) Cameron, S. G.; Schipper, L. A. Nitrate Removal and Hydraulic Performance of Organic Carbon for Use in Denitrification Beds. Ecol. Eng. 2010, 36, 1588−1595.
(26) Plötze, M.; Niemz, P. Porosity and Pore Size Distribution of Different Wood Types as Determined by Mercury Intrusion Porosimetry. Eur. J. Wood Wood Prod. 2011, 69, 649−657.
(27) Donaldson, J. H.; Istok, J. D.; Humphrey, M. D.; O'Reilly, K. T.; Hawelka, C. A.; Mohr, D. H. Development and Testing of a Kinetic Model for Oxygen Transport in Porous Media in the Presence of Trapped Gas. Ground Water 1997, 35, 270.
(28) van Genuchten, M. T. Nonequilibrium transport parameters from miscible displacement experiments. Research Report 119; U.S. Department of Agriculture, U.S. Salinity Lab. 1981.
(29) Cameron, S. G.; Schipper, L. A. Hydraulic Properties, Hydraulic Efficiency and Nitrate Removal of Organic Carbon Media for Use in Denitrification Beds. Ecol. Eng. 2012, 41, 1−7.
(30) Jaynes, D. B.; Moorman, T. B.; Parkin, T. B.; Kaspar, T. C. Simulating Woodchip Bioreactor Performance Using a Dual-Porosity Model. J. Environ. Qual. 2016, 45, 830−838.
(31) Gerke, H. H.; van Genuchten, M. T. A Dual-porosity Model for Simulating the Preferential Movement of Water and Solutes in Structured Porous Media. Water Resour. Res. 1993, 29, 305−319.
(32) Cabrol, L.; Quéméneur, M.; Misson, B. Inhibitory Effects of Sodium Azide on Microbial Growth in Experimental Resuspension of Marine Sediment. J. Microbiol. Methods 2017, 133, 62−65.
(33) Balcke, G. U.; Meenken, S.; Hoefer, C.; Oswald, S. E. Kinetic Gas-Water Transfer and Gas Accumulation in Porous Media during Pulsed Oxygen Sparging. Environ. Sci. Technol. 2007, 41, 4428−4434.
(34) Clark, J. F.; Hudson, G. B.; Avisar, D. Gas Transport below Artificial Recharge Ponds: Insights from Dissolved Noble Gases and a Dual Gas (SF_6 and ^3He) Tracer Experiment. Environ. Sci. Technol. 2005, 39, 3939−3945.
(35) Geistlinger, H.; Beckmann, A.; Lazik, D. Mass Transfer between a Multicomponent Trapped Gas Phase and a Mobile Water Phase: Experiment and Theory. Water Resour. Res. 2005, 41, W11408.
(36) Suekane, T.; Zhou, N.; Hosokawa, T.; Matsumoto, T. Direct Observation of Trapped Gas Bubbles by Capillarity in Sandy Porous Media. Transp. Porous Media 2010, 82, 111−122.
(37) Suenaga, T.; Riya, S.; Hosomi, M.; Terada, A. Biokinetic Characterization and Activities of N_2O-Reducing Bacteria in Response to Various Oxygen Levels. Front. Microbiol. 2018, 9, 697.
(38) Maxwell, B. M.; Birgand, F.; Schipper, L. A.; Christianson, L. E.; Tian, S.; Helmers, M. J.; Williams, D. J.; Chescheir, G. M.; Youssef, M. A. Drying−Rewetting Cycles Affect Nitrate Removal Rates in Woodchip Bioreactors. J. Environ. Qual. 2019, 48, 93−101.
(39) United States Department of Agriculture. Natural Resources Conservation Service Conservation Practice Standard Denitrifying Bioreactor Code 605. 2015.
(40) McClain, M. E.; Boyer, E. W.; Dent, C. L.; Gergel, S. E.; Grimm, N. B.; Groffman, P. M.; Hart, S. C.; Harvey, J. W.; Johnston, C. A.; Mayorga, E.; et al. Biogeochemical Hot Spots and Hot Moments at the Interface of Terrestrial and Aquatic Ecosystems. Ecosystems 2003, 6, 301−312.
(41) Delsontro, T.; Kunz, M. J.; Kempter, T.; Wüest, A.; Wehrli, B.; Senn, D. B. Spatial Heterogeneity of Methane Ebullition in a Large Tropical Reservoir. Environ. Sci. Technol. 2011, 45, 9866−9873.
(42) Fechner-Levy, E. J.; Hemond, H. F. Trapped Methane Volume and Potential Effects on Methane Ebullition in a Northern Peatland. Limnol. Oceanogr. 1996, 41, 1375−1383.
(43) Baulch, H. M.; Dillon, P. J.; Maranger, R.; Schiff, S. L. Diffusive and Ebullitive Transport of Methane and Nitrous Oxide from Streams: Are Bubble-Mediated Fluxes Important? J. Geophys. Res.: Biogeosci. 2011, 116, G04028.
(44) Halaburka, B. J.; Lefevre, G. H.; Luthy, R. G. Quantifying the Temperature Dependence of Nitrate Reduction in Woodchip Bioreactors: Experimental and Modeled Results with Applied Case-Study. Environ. Sci.: Water Res. Technol. 2019, 5, 782−797.
(45) Roser, M. B.; Feyereisen, G. W.; Spokas, K. A.; Mulla, D. J.; Strock, J. S.; Gutknecht, J. Carbon Dosing Increases Nitrate Removal Rates in Denitrifying Bioreactors at Low-Temperature High-Flow Conditions. J. Environ. Qual. 2018, 47, 856−864.
(46) Weiss, R. F.; Price, B. A. Nitrous Oxide Solubility in Water and Seawater. Mar. Chem. 1980, 8, 347−359.
(47) Bock, E. M.; Coleman, B. S. L.; Easton, Z. M. Effect of Biochar, Hydraulic Residence Time, and Nutrient Loading on Greenhouse Gas Emission in Laboratory-Scale Denitrifying Bioreactors. Ecol. Eng. 2018, 120, 375−383.
(48) Hassanpour, B.; Giri, S.; Pluer, W. T.; Steenhuis, T. S.; Geohring, L. D. Seasonal Performance of Denitrifying Bioreactors in the Northeastern United States: Field Trials. J. Environ. Manage. 2017, 202, 242−253.
(49) Ray, J. R.; Shabtai, I. A.; Teixido, M.; Mishael, Y. G.; Sedlak, D. L. Polymer-Clay Composite Geomedia for Sorptive Removal of Trace Organic Compounds and Metals in Urban Stormwater. Water Res. 2019, 157, 454−462.
(50) Keiluweit, M.; Nico, P. S.; Johnson, M. G.; Kleber, M. Dynamic Molecular Structure of Plant Biomass-Derived Black Carbon (Biochar). Environ. Sci. Technol. 2010, 44, 1247−1253.
(51) Robertson, W. D. Nitrate Removal Rates in Woodchip Media of Varying Age. Ecol. Eng. 2010, 36, 1581−1587.

DOI: 10.1021/acs.est.9b04829
Environ. Sci. Technol. 2019, 53, 14348−14356